Online Research @ Cardiff

This is an Open Access document downloaded from ORCA, Cardiff University's institutional repository: https://orca.cardiff.ac.uk/id/eprint/123721/

This is the author's version of a work that was submitted to / accepted for publication.

Citation for final published version:

Zheng, Shuang, Lourenço, Sérgio D.N., Cleall, Peter J. ORCID: https://orcid.org/0000-0002-4005-5319 and Ng, Angel K.Y. 2019. Erodibility of synthetic water repellent granular materials: adapting the ground to weather extremes. Science of the Total Environment 689 , pp. 298-412. 10.1016/j.scitotenv.2019.06.328 file

Publishers page: https://doi.org/10.1016/j.scitotenv.2019.06.328 <https://doi.org/10.1016/j.scitotenv.2019.06.328>

Please note:
Changes made as a result of publishing processes such as copy-editing, formatting and page numbers may not be reflected in this version. For the definitive version of this publication, please refer to the published source. You are advised to consult the publisher's version if you wish to cite this paper.

This version is being made available in accordance with publisher policies. See http://orca.cf.ac.uk/policies.html for usage policies. Copyright and moral rights for publications made available in ORCA are retained by the copyright holders.

information services
gwasanaethau gwybodaeth

Erodibility of synthetic water repellent granular materials: adapting the ground to weather extremes

Shuang Zheng[1], Sérgio D.N. Lourenço[1*], Peter J. Cleall[2], Angel K.Y. Ng[3]

[1] Department of Civil Engineering, The University of Hong Kong, Hong Kong S.A.R., China

[2] School of Engineering, Cardiff University, United Kingdom

[3] Ove Arup & Partners (Hong Kong) Ltd., Hong Kong S.A.R, China

* Corresponding author

*Manuscript (double-spaced and continuously LINE and PAGE numbered)-for final publication
Click here to view linked References

Abstract

Granular materials with synthetic water repellent coatings have great potential to be used in ground interfaces (ground-atmosphere-vegetation and ground-structure) as infiltration barriers, due to their altered hydrological properties (suppressed infiltration and decreased sorptivity). However, very few studies have evaluated the impact of synthetic soil water repellency on soil erosion. This paper investigates the effect of water repellency on soil erosional behavior, including splash erosion and rill processes. Twenty-four flume tests were carried out on model slopes under artificial rainfall; soils with three wettability levels were tested, including wettable (contact angle, CA < 90°), subcritical water repellent (CA ~ 90°) and water repellent (CA > 90°). Various rainfall intensities (230 mm/h, 170 mm/h, 100 mm/h and 40 mm/h) and grain sizes (Fujian sand and sand/silt mixture) were adopted. Erosional variables, including splash erosion rate, average sediment concentration, peak sediment concentration and time to peak sediment were measured to quantitatively analyze the behavior. This study confirms the impact of water repellency on soil erosion and unveils the possibility to reduce infiltration at ground-atmosphere interface with controlled soil erosion. The results revealed that: (1) synthetic water repellency does not necessarily lead to increased soil erosion yield; its impact is dependent on grain size with the soil erosion loss increasing for Fujian sand, but decreasing for sand/silt mixtures; (2) splash erosion is positively correlated to soil water repellency and high rainfall intensity, regardless of grain size; (3) the erosion processes for sand/silt mixtures are

particle size selective and not affected by soil water repellency, whereas this phenomenon is not observed with Fujian sand.

Keywords: Synthetic soil water repellency, flume test, soil erosion, splash erosion, particle size selectivity

1. Introduction

The influence of soil water repellency on the soil hydrological behavior has been extensively investigated, both in the natural environment and the laboratory (Mao et al., 2019). It is known to increase the water entry value (Wang et al., 2000), decrease the infiltration capacity (Doerr et al., 2006), sorptivity (Ebel and Moody, 2017), field saturated hydraulic conductivity (Fox et al., 2007) and therefore lead to promoted overland flow (Jordán et al., 2016). The distinctive hydrological properties of synthetic water repellent soils suggest that it may be utilized in the built environment, as infiltration barriers, for slope stabilization or ground improvement measures (Lourenço et al., 2018; Dell'Avanzi et al., 2010). As an important component of land degradation, soil erosion was observed to increase considerably on naturally occurring water repellent soils (Doerr et al., 2006), due to reduced infiltration and enhanced overland flow (Cerdà et al., 1998), promoted rain splash detachment of soil (Shakesby et al., 1993) and increased soil erodibility (Sheridan et al., 2007). Nevertheless, little exists on the impacts of synthetic soil water repellency on soil erosion (Mohammadi et al., 2018). For instance, synthetic soil water repellency is induced by films with a thickness in the μm range (up to 10 μm) and with physical properties that differ from natural water repellent substances. The coatings are soft and smoothen the particle surface (Liu et al., 2019). Therefore, an insight is needed on the erosional behavior of soils with synthetic water repellent coatings.

Previous research mainly focused on the interaction between raindrops and water repellent soils on small samples. Terry and Shakesby (1993) conducted a series of simulated rainfall experiments and concluded that rain splash detachment is more prominent on water repellent soil than on wettable soil. This influence of soil water repellency, either naturally occurring or chemically induced, has been confirmed by Ahn et al. (2013) and Jordán et al. (2016), revealing a greater splash distance, higher ejecting velocity and larger splash erosion rate. In laboratory experiments in synthetic water repellent sands, McHale et al. (2007) identified the formation of liquid marbles as a mechanism which promotes erosion of loose water repellent sand: water droplets which are fully covered by the soil particles and are highly mobile on sloping surfaces. Atherton et al. (2016) assessed the interaction of water drops impacting multi-layered bead packs with mixed soil wettability, and suggested that a water repellent top layer can increase splash erosion without affecting the matrix below. Wettable particles just below the surface, however, may result in multiple layers of the soil matrix eroding simultaneously. Despite past research on rain splash erosion, questions remain on the erosional impacts of soil water repellency, including different erosional processes (rill and splash erosion) and at scales greater than the previous studies.

To comprehensively assess the overall erosional impacts of soil water repellency, it is vital to separate the different types of processes. Bryan (2000) identified two distinct sub-processes of soil erosion in natural slopes: interrill and rill processes. Interrill erosion includes the detachment of soil by rain splash and following entrainment by

72 shallow surface flow, this process is primarily dominated by the kinetic energy of rain
73 splash, which can be determined by the rainfall intensity and raindrop size distribution
74 (Carollo et al., 2017). A threshold kinetic energy, which is dependent on soil properties,
75 has to be reached for a raindrop to be erosive and initiate soil dislodgement (Greene
76 and Hairsine, 2004). Rill erosion is caused by concentrated flow and not directly
77 influenced by raindrop impact, where it depends on both the flow behavior (flow
78 velocity, turbulence level etc.) and the soil's resistance to concentrated flow.
79
80 Rainfall is one of the major active agents of soil erosion, its capability to erode soil, i.e.
81 rainfall erosivity is closely related to the rainfall characteristics (rainfall intensity,
82 duration, kinetic energy etc.) (van Dijk et al., 2002). In RUSLE (Revised Universal Soil
83 Loss Equation, Renard et al., 1991), rainfall erosivity is calculated by multiplying the
84 kinetic energy of the rainfall by the maximum continuous 30-min intensity in the event.
85 A soil's resistance to erosion, or soil erodibility is strongly dependent on soil properties,
86 including grain size, initial moisture content, shear strength, aggregate stability,
87 organic matter content, etc. (Knapen et al., 2007; Sheridan et al., 2000). Ayoubi et al.
88 (2018a) evaluated soil properties affecting soil loss in central Iran, indicating that soil
89 erodibility indices (runoff volume, soil loss, and sediment concentration) showed
90 positive and significant correlations with bulk density and negative correlations with
91 mean weight diameter, soil organic carbon, clay content and soil shear strength. The
92 spatial pattern of soil redistribution rate was explored using the Cs-137 technique
93 (Afshar et al., 2010; Ayoubi et al., 2012; Rahimi et al., 2013), demonstrating the

effects of human activities and land use on soil erosion.

This paper attempts to evaluate the erosional behavior of soils with artificially induced water repellency, to facilitate the utilization of synthetic water repellent soils in the built environment, by means of model granular materials and under laboratory-controlled conditions. No roots, organic matter and vegetative ash were involved. The specific objectives of the study are: (1) to evaluate the influence of water repellency on splash erosion and the initiation of rill erosion; (2) to investigate the interaction effect between water repellency and grain size on soil erosion, and (3) to elucidate the different mechanisms involved.

2. Materials and Methods

2.1. Soil description

As sands are cohesionless and easily erodible granular materials, and soil erodibility was reported to decrease with the decrease in silt fraction (Wischmeier and Mannering, 1969), two model (or mineral) soils with different grain size distributions are adopted in this paper: Fujian sand (China ISO standard sand) and crushed silica (silt). The erosional behavior of these two soils are expected to be different. Fujian sand is a clean, siliceous sand consisting preferably of rounded particles with a silica content ≥ 98%. Its particle size distribution complies with ISO 679:2009, as displayed

116 in Fig. S1, and is classified as poorly graded sand. Crushed silica has the same
117 composition as Fujian sand, and is crushed with a median size of 20 μm (silt). The
118 grain size distribution of crushed silica is obtained using a particle size and shape
119 analyzer (QICPIC, Sympatec GmbH, Germany) and presented in Fig. S1 as well. The
120 physical properties of Fujian sand and crushed silica are summarized in Table 1. The
121 specific gravity, coefficient of uniformity and coefficient of curvature were determined
122 following BS 1377-2 (British Standards Institution, 1990). The organic matter content
123 was determined via loss on ignition (LOI) analysis (BS 1377-3), by heating the
124 sub-samples at 450 °C for 1 hour. The maximum void ratio and minimum void ratio
125 were determined by following the procedures in BS 1377-4.
126
127 *2.2. Soil silanization*
128
129 The occurrence of soil water repellency normally results from the presence of water
130 repellent coatings around the soil particles. Dimethyldichlorosilane (DMDCS) has
131 been widely used in previous studies (Bachmann et al., 2000; Ng and Lourenço, 2016)
132 as a hydrophobizing agent to artificially induce water repellency in soil samples. The
133 treatment is based on silanization, by reaction between DMDCS and residual water,
134 polydimethylsiloxane (PDMS) is formed and bonded to the soil particle surface along
135 with the formation of HCl gas as a by-product. The level of water repellency is
136 dependent on the DMDCS concentration and soil type. Zheng et al. (2017) treated the
137 natural completely decomposed granite with 3% of DMDCS by soil mass to attain a

138 CA of 115°. Ng and Lourenço (2016) found that the maximum CA can be induced
139 using 3% and 0.005% DMDCS by soil mass for alluvium and Leighton Buzzard sand,
140 respectively. For Fujian sand and crushed silica, the critical DMDCS concentrations to
141 reach the maximum CA are 0.1% and 0.2% respectively, as indicated by Fig. S2. To
142 allow soil water repellency to establish and for consistency among the tests, the
143 materials were treated and equilibrated at ambient air conditions for 3 days before
144 using.
145
146 *2.3. Soil water repellency assessment*
147
148 Materials of various water repellency levels were used in this study, and the water
149 repellency level of soil samples was assessed with two measuring techniques: sessile
150 drop method (SDM) and water drop penetration time (WDPT).
151
152 The SDM is a direct method to measure the CA of water drop on a soil sample surface
153 (Bachmann et al., 2000). When a drop of water is dispensed on a surface, the
154 three-phase contact line between the soil, water, and air will move in response to the
155 three interfacial tensions, forming a CA which is a direct quantification of soil
156 wettability. The CA of a wettable soil and water repellent soil is < 90° and > 90°
157 respectively, and a subcritical water repellent soil has a CA ~ 90°, which is generally
158 regarded as a wettability boundary between wettable and water repellent conditions.
159 The CA measurement procedures were introduced by Bachmann et al. (2000) and

improved by Saulick et al (2017) as follows: (1) the soil is sprinkled on a double-sided adhesive tape fixed on a glass slide, and by removing the excess particles to ensure a monolayer of particles is fixed; (2) placing the slide on a goniometer's (DSA 25, KRÜSS GmbH, Germany) sample stage and dispensing a droplet of deionized water (10 µL) onto the sample; (3) contact angle measurements are then performed by analyzing the shape of the droplet on the soil surface. Six drops were applied to the surface of each soil sample.

WDPT is an index test that evaluates the persistence of water repellency of a soil sample (Doerr, 1998). The test is conducted by placing a drop of deionized water (50 µL, same as in Leelamanie et al., 2008) on the surface of prepared soil sample and recording the time taken for the water drop to completely infiltrate (Doerr, 1998). For wettable soils, the water drop should penetrate within 5 s (Bisdom et al., 1993), and for water repellent soils, the stronger the water repellency the longer the penetration time. Based on the WDPT, the water repellency of soils can be classified into different categories, from wettable to extremely water repellent. For each soil sample, the WDPT of 6 drops were measured.

3. Flume tests

3.1. Flume configuration

182 Flume tests have been widely adopted to investigate the hydrological and geomorphic
183 behavior of various types of soils under artificial rainfall (Bryan and Poesen, 1989; Shi
184 et al., 2017). In this paper, a perspex-sided flume was manufactured to carry out the
185 experiments, and the dimensions of the slope model were 80 cm long, 40 cm wide
186 and 5 cm deep. To facilitate the collection of water and eroded sediment, a collection
187 system was installed at the downslope edge of the flume. Sandpaper (Simax
188 LPE-22-4) was glued on the base of the flume to provide friction, and a permeable
189 baffle was installed at the toe to prevent the model slope from sliding at the soil-flume
190 interface, while water was allowed to drain through. A rainfall simulation system was
191 installed to generate the desired rainfall intensities (40, 100, 170 and 230 mm/h). The
192 system consisted of a nozzle (FullJet, Spraying Systems, US), a flowmeter and a
193 control valve to ensure constant rainfall intensity during tests. Two FDR (frequency
194 domain reflectometry) moisture sensors (EC-5, Decagon Devices, US) were buried at
195 the same depth (4 cm), one near the slope toe and the other near the crest to track
196 the wetting front movement. A video camera (HERO4 Silver, GoPro, US) was
197 positioned above the slope surface to record surface morphology evolution. Fig. 1
198 shows the configuration of the flume and instrumentation.
199
200 *3.2. Model preparation and test procedures*
201
202 The model was filled with the dry soil in a horizontal orientation (i.e. slope angle of
203 zero) into 5 layers with a thickness of 1 cm, no compaction was applied to make sure

204 the soils were in loose state and readily erodible, with the minimum bulk density of
205 1.77 g/cm^3 achieved. The slope surface was smoothed by a wooden block to help
206 eliminate differences in surface conditions among experiments, then the flume was
207 inclined to a slope angle of 10°.
208
209 The data logger, camera and stopwatch were synchronized before the experiments
210 began and started recording once the rainfall simulator was activated. Each
211 experiment lasted for 120 minutes, as preliminary testing indicated that the steady
212 state condition was achieved within 120 minutes. The wetting behavior or spatial
213 evolution of water content was traced by the FDR moisture sensors. The runoff and
214 eroding sediment were collected by a container at the slope toe at 5-min intervals
215 (2-min intervals for high rainfall intensities). In this study, the term “runoff” not only
216 implies overland flow but also includes subsurface flow that eventually flows out of the
217 flume (for wettable soils). In this context, the runoff is equivalent to the difference
218 between rainfall intensity and water stored in soil mass and equals to the rainfall
219 intensity when the steady state (near-saturation) is reached. After the rainfall event,
220 the collected sediment was oven dried to determine the mass of water, sand and silt
221 (if present) for further analysis. Particle size distribution analysis was carried out for
222 samples obtained at each collecting interval.
223
224 *3.3. Testing program*
225

To investigate the influence of soil wettability, grain size and rainfall intensity on soil erosion, a factorial design of flume tests involving these three factors was used in this study. A total of 24 flume tests were conducted and are listed in Table 2. Four rainfall intensities (40, 100, 170 and 230 mm/h) were selected to cover a wide range of rainfall scenarios, the exceptional ones were adopted to compensate for the influence of smaller raindrop velocity and achieve a high enough kinetic energy. Two different grain sizes: Fujian sand and 50/50 sand/silt mixture (silt is crushed silica) were selected, to examine the effect of grain size on soil erosion under wettable and water repellent conditions. The tests were not repeated, as the model materials were adopted, with the initial condition (e.g. dry density, slope angle etc.) well controlled, all sensors and nozzles were calibrated before conducting experiments.

Following Zheng et al. (2017), three water repellency levels were selected based on the CA and WDPT achieved. For wettable soils, no treatment was applied and the CA and WDPT were lowest (CA = 20.3 ± 2.6° for Fujian sand and 71.1 ± 5.3° for crushed silica; WDPT = 0 s). The different CAs between Fujian sand and crushed silica was a result of changing particle size, as the CA increased with decreased particle size (Saulick et al., 2018). The critical DMDCS concentrations were used for the treatment of water repellent soils, i.e. 0.1% and 0.2% for Fujian sand and crushed silica respectively, with the maximum CA and WDPT > 3600 s attained (Fig. S2). For subcritical water repellent conditions, the concentrations of DMDCS adopted for Fujian sand and crushed silica were 0.05% and 0.1%, respectively, with the CA of ~

248 90° achieved.

249

250 *3.4. Soil splash test*

251

252 To determine the soil splash erosion rate, 24 soil splash tests were carried out under
253 the same conditions as the flume tests (rainfall intensity, CA and grain size). A similar
254 set-up as in Jordán et al. (2016) was adopted. For each test, six splash cups (5.5 cm
255 radius) filled with dry soil were prepared and the mass weighed. Then the cups were
256 placed under the spraying nozzle and subjected to 30-min rainfall at the designated
257 rainfall intensity, subsequently, the remaining soil was oven dried and weighed to
258 determine the splash erosion rate.

259

260 *3.5. Data analysis*

261

262 To quantitatively analyze the raw data obtained from the tests, a series of variables
263 were defined as follows:

264

265 • Splash erosion rate (E_s, g/mm): The mass of soil splash loss divided by the
266 rainfall depth (as defined in Terry and Shakesby, 1993);
267 • Average sediment concentration (S_a, g/L): Total mass of sediment in runoff
268 divided by the total volume of runoff throughout the experiment; total mass of
269 sediment is also calculated and plotted as a reference (as defined in Asadi et

al., 2011);

- Peak sediment concentration (S_p, g/L): The maximum sediment concentration in a 5-min interval (2-min for high rainfall intensity conditions);
- Time to peak sediment (T_p, minute): The time when maximum sediment concentration is recorded; time to peak runoff is also recorded and plotted as a reference.

3.6. Statistical analysis

Statistical analyses were performed using Real Statistics Resource Pack software (Release 5.4, Zaiontz, 2018) and MATLAB (R2014b, MathWorks, US). A factorial analysis of variance (ANOVA) followed by a Tukey's HSD test was conducted to examine statistically significant differences (level of significance = 0.05) in the values of variables from different experiments. Regression analysis (Tajik et al., 2012; Ayoubi et al., 2018b) was adopted to characterize the relationships between rainfall intensity, CA and soil erosion variables. The best-fitting equations all 4 variables were presented for Fujian sand and sand/silt mixture separately. A correlation matrix of the Pearson correlation coefficients was obtained to analyze the correlations between rainfall intensity, wettability level and soil erosional parameters (level of significance = 0.05).

4. Results

To describe the typical hydrological and erosional responses, the time series data were analyzed and presented, including runoff rate, sediment concentration, volumetric water content and surface morphology. Based on the wettability level and grain size, the tests were classified into 5 groups, i.e. (1) wettable and subcritical water repellent sand, (2) water repellent sand, (3) wettable sand/silt mixture, (4) subcritical water repellent sand/silt mixture and (5) water repellent sand/silt mixture. Due to large number of tests, five tests (one from each group) were analyzed and presented in Fig. 2-6. The soil erosional variables of each test were summarized in Table 2 and Fig. 7, where the time to peak sediment, average sediment concentration, peak sediment concentration, total mass of sediment and time to peak runoff of Fujian sand and sand/silt mixture were presented separately, due to the contrasting behavior between the two grain sizes. In addition, Fig. 8-9 compared the results among tests and examine the impacts of grain size, rainfall intensity and soil wettability. The splash erosion rate and the sediment particle size distribution analysis were shown in Fig. 8 and Fig. 9, respectively.

4.1. Temporal evolution of erosion

4.1.1. Wettable and subcritical water repellent sand

313 Test 7 (Fujian sand, CA = 20°, rainfall intensity = 170 mm/h) shows the typical
314 hydrological and erosional responses, with the results presented in Fig. 2. At the
315 rainfall onset, all rainwater infiltrated and no surface runoff was observed (Fig. 2a).
316 The wetting front was parallel to the surface and the moisture sensor readings
317 remained unchanged (Fig. 2b). At 2 min, a sudden rise in volumetric water content
318 was recorded by both sensors 1 and 2, implying that the wetting front had reached the
319 sensors (4 cm deep). Subsequently, a jump in runoff rate occurred at 4 min until a
320 steady state was reached at 8 min (Fig. 2a), i.e. all rainwater converted into runoff with
321 the runoff rate becoming equal to the rainfall intensity. The volumetric water content
322 increased to 28.5% at steady state (Fig. 2b), with the volumetric water content at
323 saturation was 34.5%.
324
325 As for the soil erosional behavior, the sediment concentration at each sampling
326 interval was calculated. The sediment concentration experienced a drop (from 6.7 to
327 0.6 g/L) after the test began, which was a result of the substantially increased runoff
328 rate (from 3.4 to 177.8 mm/h), although the sediment mass barely changed at this
329 stage. After the steady state was reached, the entrainment and transportation of
330 particles by surface runoff dominated the erosional processes. With the development
331 of surface flow and rill erosion (Fig. 2c), the erosivity of the concentrated flow in the
332 rills increased and subsequently the sediment concentration started to show a sharp
333 rise until the peak sediment concentration was recorded at 20 min. For wettable and
334 subcritical water repellent sand, the increase in rainfall intensity led to decreased time

335 to peak sediment (Fig. 7a), whereas the average sediment concentration (Fig. 7c) and
336 peak sediment concentration (Fig. 7e) were positively influenced by rainfall intensity.
337 The time to peak sediment was shortened from 120 min (under 40 mm/h rainfall) to 15
338 min (under 230 mm/h rainfall). The average sediment concentration was 0.0 g/L at the
339 rainfall intensity of 40 mm/h, implying that a higher rainfall intensity was necessary to
340 initiate erosion, while the average sediment concentration and peak sediment
341 concentration under 230 mm/h rainfall were 47.75 g/L and 89.67 g/L, respectively.
342
343 4.1.2. Water repellent sand
344
345 The results of test 3 (Fujian sand, CA = 120°, rainfall intensity = 230 mm/h) were
346 presented in Fig. 3. Infiltration was suppressed regardless of the rainfall intensity, with
347 the steady state runoff achieved at the beginning of test (Fig. 3a). The volumetric
348 water content remained constant throughout the test (Fig. 3b), indicating that no
349 infiltration occurred, an observation that is supported by the measured runoff rate.
350
351 As a result of enhanced overland flow, concentrated flow-driven soil erosion increased
352 substantially. The peak sediment (236.2 g/L) was recorded at the commencement of
353 the rainfall event, followed by a gradual decrease until reaching an approximately
354 constant level (45 g/L), which was greater than that of the wettable and subcritical
355 water repellent soil. Besides increased soil erosion, the surface morphology of water
356 repellent sand showed unique characteristics during the test. At the onset of the test,

357 erosion processes were dominated by rainsplash, as the sand particles were dry,
358 loose and readily detachable. Due to the presence of water repellency, the infiltration
359 of rainwater was suppressed with surface runoff appeared promptly. The sand
360 particles were then entrained by the downward surface runoff, causing localized
361 erosion, which formed a series of “steps” or cascades on the surface, as recorded in
362 Fig. 3c. As the erosion processes continued, the eroded zones expanded and merged,
363 with three major rills formed. The positive impacts of rainfall intensity on the erosional
364 variables of water repellent sand were revealed by Fig. 7. Higher rainfall intensity
365 resulted in reduced time to peak sediment (from 60 min to 5 min, Fig. 7a), as well as
366 increased average sediment concentration (from 2.25 g/L to 94.8 g/L, Fig. 7c) and
367 peak sediment concentration (from 3.57 g/L to 236.19 g/L, Fig. 7e), when the rainfall
368 intensity increased from 40 mm/h to 230 mm/h.
369
370 4.1.3. Wettable sand/silt mixture
371
372 The results of representative wettable sand/silt mixture are shown in Fig. 4 (test 16:
373 mixture, CA = 20°, rainfall intensity = 100 mm/h). The steady state was reached at 20
374 min, with the soil in a near saturation state (degree of saturation 90%). The sediment
375 concentrations of sand and silt experienced similar changes (Fig. 4a), no erosion was
376 recorded during the first 5 min of the experiment. At 10 min, a sudden rise in
377 volumetric water content was simultaneously recorded by sensor 1 and 2 (Fig. 4b).
378 Accompanied by the sharp increase in water content and runoff at 10 min,

379 concomitant growth in sand and silt sediment concentration was recorded, which
380 reached the peak sediment concentration (139.6 g/L for silt and 121.5 g/L for sand) at
381 20 min. Similar to other experiments, the sediment concentration reduced after the
382 peak till the end of the test. Cracks appeared within the first 5 min of a rainfall event,
383 as illustrated in Fig. 4c, which is a unique surface morphology characteristic that was
384 not observed in other conditions. It is assumed that the cracks may result from
385 localized variations in stress and strain conditions, and subsequent developments of
386 tensile stresses that lead to crack initiation. After the formation of cracks in the soil
387 surface, sand and silt particles were dislodged from the cracks and micro rills
388 developed. Owing to the imposed boundary conditions, surface runoff concentrated
389 on the sides of the flume and two major rills were formed at these locations within 20
390 min. Within the group of wettable sand/silt mixture tests (Fig. 7), the average sediment
391 concentration decreased from 83.49 g/L (40 mm/h) to 74.05 g/L (230 mm/h) (Fig. 7d)
392 and the peak sediment concentration dropped from 302.95 g/L (40 mm/h) to 160.81
393 g/L (230 mm/h) (Fig. 7f). The decreased sediment concentration does not imply less
394 soil erosion, but the increase in runoff was greater than the increase in erosion.
395
396 4.1.4. Subcritical water repellent sand/silt mixture
397
398 As can be seen in Fig. 5a, and unlike the subcritical water repellent sand test,
399 infiltration of rainwater was impeded in test 23 (mixture, CA = 90°, rainfall intensity =
400 40 mm/h). Preferential flow, instead of a parallel wetting front, was observed. The

readings of sensor 1 and 2 remained unchanged at the beginning until 30 min (Fig. 5b), implying the preferential flow reached the sensors. Development of runoff was initially delayed and then followed by a sharp increase at 5 min and then a gradual increase with steady state reached after 65 min. At the end of the test (after 120 min), the degree of saturation was only 57%. The sediment concentration was 0.0 g/L for sand throughout the test, whereas eroded silt particles had a peak sediment concentration of 17.9 g/L, suggesting that higher rainfall intensity is needed to initiate the erosion of sand particles, owing to greater particle mass.

Due to the relatively low rainfall intensity and sediment concentration of test 23 (40 mm/h), negligible change in surface morphology was observed. Therefore, test 5 (230 mm/h) was selected and four photos showing the surface morphology change were exhibited in Fig. 5c. Unlike the wettable condition, no cracks were observed on the soil surface. Rainsplash induced circular depressions appeared after the experiment began, along with the development of surface runoff, the circular depression gradually expanded and evolved into rills. It is worth noting that the surface became rougher on eyesight with time, as a result of unequal erosion severity of coarse and fine particles. The fine particles were easily eroded while the coarse particles remained, causing a rougher surface at the end of the experiment. The increased rainfall intensity had positive influence on erosional variables of subcritical water repellent sand/silt mixture (Fig. 7). With the increase in rainfall intensity from 40 mm/h to 230 mm/h, the time to peak sediment decreased from 15 min to 2 min (Fig. 7b), whereas the average

423 sediment concentration grew from 6.37 g/L to 28.45 g/L (Fig. 7d) and the peak
424 sediment concentration increased from 17.85 g/L to 89.01 g/L (Fig. 7f).
425
426 4.1.5. Water repellent sand/silt mixture
427
428 Test 6 (mixture, CA = 90°, rainfall intensity = 230 mm/h) was the representative test
429 and the results were presented in Fig. 6. Immediately after the onset of rainfall,
430 overland runoff appeared on the surface (Fig. 6a), in the form of liquid marbles, i.e.
431 water drops which rolled on the water repellent surface with a powder coating. No
432 infiltration occurred throughout the 120 min rainfall (Fig. 6b, unchanged readings of
433 sensor 1 and 2). Steady state was reached at 4 min, after a water film was formed on
434 the soil surface. At the same time, the maximum sediment concentration of sand and
435 silt grains was reached, with a sediment concentration of 32.4 g/L and 41.7 g/L
436 measured respectively (Fig. 6b). As the rainfall continued, localized erosion was
437 observed on the soil surface (“scars” in Fig. 6c). Subsequently, the dry soil beneath
438 was exposed to surface flow and eroded, with the eroded zones expanding till the end
439 of the experiment. When subjected to increased rainfall intensity (from 40 mm/h to
440 230 mm/h), the time to peak sediment was shortened from 15 min to 4 min (Fig. 7b),
441 whereas the average and peak sediment concentration increased from 6.58 g/L to
442 20.91 g/L (Fig. 7d) and from 20.22 g/L to 74.12 g/L (Fig. 7f), respectively.
443

4.2. Soil splash erosion

The splash erosion rate of all experiments was summarized in Fig. 8, the box and whisker plots were adopted for clear comparison. The splash erosion rate increased from wettable to subcritical water repellent to water repellent. However, the splash erosion rates of water repellent soils had a greater standard deviation, indicating potential variations in splash erosion severity at different locations. Rainfall intensity, in comparison to soil water repellency, had a minor influence on soil splash erosion. Within each wettability level, the splash erosion rate increased when subjected to higher rainfall intensity, both for sand (Fig. 8a) and sand/silt mixture (Fig. 8b) conditions. There was no significant difference observed between the mean splash erosion rates of sand and sand/silt mixture, suggesting that splash erosion was not sensitive to grain size change.

4.3. Particle size distribution of eroded sediment

To investigate the dynamic changes in sediment particle size distribution, analysis was conducted with collected sediment at each time interval for each experiment. Commonly used particle size distribution parameters were calculated, including D_{10} (diameter of soil particles for which 10% of the particles are finer, similarly for D_{30} and D_{60}), D_{30}, D_{60}, C_u (uniformity coefficient, defined as D_{60}/D_{10}) and C_c (coefficient of curvature, defined as $D_{30}^2/(D_{60}\times D_{10})$). All parameters showed similar trends and D_{60}

experienced the greatest change, therefore only the temporal evolution in D_{60} was presented. Fig. 9a illustrated that the grain size distribution of eroding sediment for sand barely changed with time, which was similar to the original soil throughout the test, indicating that the erosion processes of sand were not size selective. A representative test (test 3: Fujian sand, CA = 120°, rainfall intensity = 230 mm/h) was highlighted to show the typical trend. On the contrary, a significant change in sediment size distribution of sand/silt mixture was recorded (Fig. 9b). The D_{60} at the commencement of experiments (0.063 mm) was much smaller than that of the original soil (0.187 mm), followed by an increase until the D_{60} approximately equals to the original value. A representative test (test 5: mixture, CA = 90°, rainfall intensity = 230 mm/h) was highlighted to show the typical trend. This dynamic change in sediment size distribution suggests that the collected sediment at the early phase was dominated by silt-sized particles. With the increased runoff rate, the transport of sand particles was gradually activated, leading to a coarser sediment until the sediment particle size distribution became similar to the original soil.

4.4. Regression analysis

For all obtained best-fitting equations, the independent variables (rainfall intensity and CA) were normalized by its mean and standard deviation before curve fitting. Therefore, the size of regression coefficients indicates the size of the effect that an independent variable has on the dependent variable, i.e. the larger the coefficient, the

488 greater the effect of that term. The sign on the coefficient suggests the direction of the
489 effect (positive or negative).
490
491 The best-fitting equations of splash erosion rate for Fujian sand (Eq. 1) and sand/silt
492 mixture (Eq. 2) are in the form:

493 (1)

494 (2)

495 where E_s denotes splash erosion rate. The fitting equations of average sediment
496 concentration are obtained for Fujian sand and sand/silt mixture in Eq. 3 and 4 as
497 follows:

498 (3)

499 (4)

500 where S_a denotes average sediment concentration. The peak sediment concentration
501 for Fujian sand and sand/silt mixture were described by the Eq. 5 and 6 respectively:

502 (5)

503 (6)

where S_p denotes peak sediment concentration, and the signs of coefficients of were opposite between Fujian sand and sand/silt mixture. The time to peak sediment is fitted by CA and rainfall intensity in the form below (Eq. 7 for Fujian sand and Eq. 8 for sand/silt mixture):

(7)

(8)

where T_p denotes time to peak sediment. The correlation matrix of the Pearson correlation coefficients for CA, rainfall intensity and erosional variables was displayed in Table 3.

5. Discussion

5.1. Effect of soil water repellency

Soil water repellency has been found to promote splash erosion and accelerate surface erosion. Splash erosion rate showed a significant increase with the water repellency level (Fig. 8), from 0.01-0.10 g/mm (wettable soils) to 0.12-0.41 g/mm (water repellent soils), as suggested by Eq. 1-2. The results were in accordance with those previously reported in the literature (Fox et al., 2007; Ahn et al., 2013; Jordán et al., 2016) with water repellent soils exhibiting greater soil particle detachment caused

524 by rain splash, regardless of the origin of water repellency (naturally occurring or
525 chemically induced), grain size (coarse-grained or fine-grained), and raindrop
526 characteristics (single raindrop or simulated rainfall). The time to peak sediment was
527 sensitive to wettability change as it shortened with increased CA, from 20-120 min for
528 wettable soils to 4-60 min for water repellent soils (Fig. 7a and 7b). In addition, the
529 peak sediment concentration always occurred after the onset of surface runoff,
530 implying that concentrated overland flow is the dominant mechanism controlling
531 surface erosion.
532
533 *5.2. Interaction effect between soil water repellency and grain size*
534
535 An interaction effect between soil water repellency and grain size on sediment yield
536 was identified, demonstrated by the following two variables: average sediment
537 concentration and peak sediment concentration. Fig. 7c and 7d showed that the
538 average sediment concentration increased from wettable sand (0-47.75 g/L) to water
539 repellent sand (2.25-105.64 g/L), but decreased for sand/silt mixture, from
540 74.05-108.95 g/L for the wettable to 5.83-20.91 g/L for the water repellent. The
541 opposite signs of coefficients of between Eq. 3 and 4 indicate that the effect of
542 soil wettability differs for different grain sizes. The same trend was observed for the
543 peak sediment concentration (Fig. 7e and 7f), which increased from 0-75.78 g/L to
544 3.57-236.19 g/L for sand but declined from 160.81-302.95 g/L to 20.22-74.12 g/L for
545 sand/silt mixture (Eq. 5 and 6). The variation in results between Fujian sand and

546 sand/silt mixture may be attributed to different erosion mechanisms. For Fujian sand,
547 the concentrated overland flow is the dominant mechanism controlling erosion, which
548 is positively influenced by water repellency. For sand/silt mixture, erosion is controlled
549 by both overland flow and subsurface flow, as stated in Fox and Wilson (2010). When
550 soil water repellency is present, infiltration as well as the subsurface flow is inhibited,
551 leading to a reduction in sediment concentration. Similar results were also reported in
552 Larsen et al. (2009), where artificial rainfall was applied on both a granitic soil and a
553 micaceous soil collected from burned hillslopes (water repellent), and the influence of
554 water repellency was found to be sensitive to the soil type, with higher runoff
555 coefficient and lower sediment concentration observed on the granitic soil. Erosional
556 impacts of soil water repellency were also investigated in the field. Osborn et al. (1964)
557 compared soil loss on newly burnt, water repellent chaparral soils and plots treated
558 with wetting agents and documented that sediment yields on the untreated plots were
559 almost 14 times higher than on treated counterparts. Consistent conclusions were
560 drawn by applying simulated rainfall with clean water and surfactant-treated water (to
561 eliminate water repellency) on burned slopes (WDPT > 5 h), with the sediment yield
562 increasing by 23 times when water repellency was present (Leighton-Boyce et al.,
563 2007).
564
565 When comparing the sediment loss between sand and sand/silt mixture under water
566 repellent conditions, the average and peak sediment concentration of water repellent
567 sand was much greater (Fig. 7c-7f). It is speculated that this difference may result

568 from a contrasting surface topography, e.g. microtopographic roughness, where two
569 quite different flow regimes can be defined depending on the height of the roughness
570 elements (Fig. 10). Powell (2014) and Bryan (2000) proposed that for smooth surface
571 (sand/silt mixture), the roughness elements (silt particles) are entirely submerged by
572 the laminar sublayer and the erosive force is resisted by the complete bed surface,
573 such a flow is said to be hydraulically (or dynamically) smooth, with the boundary
574 Reynolds number < 3.5. However, for a rough surface (Fujian sand), the
575 roughness elements (sand particles) penetrate the laminar sublayer, causing a
576 hydraulically rough flow with the erosive force concentrated on and resisted by the
577 roughness elements, eventually leading to a greater soil erosion. The Pearson
578 correlation analysis (Table 3) also supported the statement that the impacts of water
579 repellency and rainfall intensity differ between Fujian sand and sand/silt mixture.
580
581 *5.3. Effect of grain size*
582
583 Fig. 9 summarizes the temporal change in sediment size distribution of sand and
584 sand/silt mixture separately and reveals that grain size plays an important role in the
585 size selectivity of sediment. The grain size distribution for sediment of Fujian sand
586 barely changes with time, whereas for sand/silt mixture, the collected sediment is
587 enriched with silt-sized particles at the beginning of experiments and gradually
588 becomes coarser, until the similar distribution as the original soil is approached. The
589 sediment size selectivity in flow-driven soil erosion processes was also observed by

590 Asadi et al. (2011), and two erosion mechanisms involved were explained.
591 Suspension-saltation (fine particles are carried by water flow or bounce along the
592 slope surface) is assumed to be the main erosion mechanism at the commencement
593 of experiments, only silt particles are affected. With the increase of runoff rate, a bed
594 load transport driven mechanism is suggested with coarse particles rolling on the
595 surface.
596
597 In addition, the effect of grain size on wettable soils agreed with Fox and Wilson (2010)
598 and Torfs et al. (2000). Average sediment concentration and peak sediment
599 concentration of sand/silt mixtures were much greater than those of Fujian sand,
600 which increased from 0-47.75 g/L to 74.05-108.95 g/L, and from 0-75.78 g/L to
601 160.81-302.95 g/L, respectively (Fig. 7c-7f). During the experiments of wettable
602 sand/silt mixture, subsurface flow was observed from the transparent flume sides,
603 which was a major contributor to the greater sediment yield. Subsurface flow can lead
604 to increased soil erosion on wettable soils through coupled mechanisms, including
605 hydraulic gradient forces that reduce the resistance of the particle to dislodgment from
606 the soil matrix and particle mobilization when soil particles are entrained in the
607 exfiltrating water.
608
609 *5.4. Effect of rainfall intensity*
610
611 Splash detachment has been reported to depend on the rainfall kinetic energy

612 (Nearing et al., 2017), which can be determined by the rainfall intensity and raindrop
613 size, and this conclusion is further supported by this study (the corresponding rainfall
614 kinetic energy of four rainfall intensities in this study are 235.2, 588.0, 999.6 and
615 1352.4 J/m^2/h, respectively). Fig. 8 showed that the splash erosion rate increased
616 with rainfall intensity for the same wettability level, although soil water repellency has
617 a dominant impact on the splash erosion rate whereas rainfall intensity has only a
618 minor contribution. For rainfall to initiate erosion processes, thresholds of particle
619 detachment or transport need to be exceeded (Greene and Hairsine, 2004). This
620 study found that the erosion thresholds are influenced by soil water repellency and
621 grain size. Fig. 7c and 7e show that the sediment concentration of wettable Fujian
622 sand subjected to 40 mm/h rainfall is 0.0 g/L, while sediment was collected for the
623 water repellent sand at the same rainfall intensity. It is also noticed that the erosion
624 threshold of sand particles is greater than silt, considering that only silt is contained in
625 the sediment in test 23 (mixture, CA = 90°, rainfall intensity = 40 mm/h, Fig. 5a).
626 Sharma et al. (1991) also concluded that the threshold kinetic energy of raindrop
627 needed to initiate soil detachment is grain size dependent, with sandy and loam soil
628 reported to have a smaller threshold. Fig. 7c-7f also showed that with an increase in
629 rainfall intensity from 40 mm/h to 230 mm/h, higher average and peak sediment
630 concentrations were observed, with an exception of wettable sand/silt mixture (Fig. 7d
631 and 9f), implying the influence of rainfall intensity is minor compared with that of grain
632 size.
633

5.5. Experimental considerations and implications

The lower end of the flume was narrower than the upper part, to facilitate the collection of eroded material. However, this set-up has caused concentrated flow and greater soil erosion. In this study, surface runoff and subsurface flow were not separated due to experimental constraints. As the impact of soil water repellency on them might be different, it would be beneficial to collect the subsurface and overland flows separately. In addition, a video camera was used to record the surface morphology change in this study, which only provided qualitative information. To quantitatively analyze the evolution in micro-topography of soil surface, terrestrial laser scanner could be adopted.

Synthetic water repellent soils have been regarded as promising materials to be utilized in the built environment as infiltration barriers, however the erosion yields of these materials need to be controlled to guarantee a satisfactory performance. At this stage and given the preliminary nature of this study, we cannot provide guidelines or firm recommendations on their use. Our findings imply that infiltration can be reduced in synthetic water repellent soils without amplifying erosion by taking grain size into consideration. In particular, the results suggest that finer soils are more appropriate because they are less prone to erosion while maintain water repellency, and therefore reveal potential for use in the built environment.

6. Conclusions

Twenty-four flume tests under artificial rainfall at various soil wettability levels, grain sizes and rainfall intensities were conducted to isolate and investigate the impact of soil water repellency on soil erosion processes. The results reveal that: (1) soil water repellency does not necessarily lead to increased soil erosion, its impact on erosion is dependent on grain size and the erosion processes involved. (2) There is a statistically significant positive correlation between splash erosion and soil water repellency, indicating that greater rain splash can be expected on synthetic water repellent soils, regardless of grain size. Higher rainfall kinetic energy also contributes to promoted splash erosion, with relatively minor influence. (3) Particle size distribution of eroded sediment is sensitive to grain size and insensitive to soil water repellency. No variation in sediment particle size distribution is observed with the Fujian sand, whereas the eroded sediment of sand/silt mixture gradually becomes coarser until reaching a similar distribution to the original soil. These findings imply that infiltration can be reduced in synthetic water repellent soils without amplifying erosion by taking grain size into consideration.

Acknowledgments

This research is financially supported by the Research Grants Council of Hong Kong (grant No. 17205915 and T22-603/15-N). Laboratory assistance by Mr. N. C. Poon

678 and Mr. Jiejia Yao is acknowledged.

References

Afshar, F. A., Ayoubi, S., & Jalalian, A. (2010). Soil redistribution rate and its relationship with soil organic carbon and total nitrogen using 137Cs technique in a cultivated complex hillslope in western Iran. Journal of Environmental Radioactivity, 101(8), 606-614.

Ahn, S., Doerr, S. H., Douglas, P., Bryant, R., Hamlett, C. A. E., McHale, G., . . . Shirtcliffe, N. J. (2013). Effects of hydrophobicity on splash erosion of model soil particles by a single water drop impact. Earth Surface Processes and Landforms, 38(11), 1225-1233.

Asadi, H., Moussavi, A., Ghadiri, H., & Rose, C. W. (2011). Flow-driven soil erosion processes and the size selectivity of sediment. Journal of Hydrology, 406(1), 73-81.

Atherton, S., Polak, D., Hamlett, C. A. E., Shirtcliffe, N. J., McHale, G., Ahn, S., . . . Newton, M. I. (2016). Drop impact behaviour on alternately hydrophobic and hydrophilic layered bead packs. Chemical Engineering Research and Design, 110, 200-208.

Ayoubi, S., Ahmadi, M., Abdi, M. R., & Afshar, F. A. (2012). Relationships of 137Cs inventory with magnetic measures of calcareous soils of hilly region in Iran. Journal of Environmental Radioactivity, 112, 45-51.

Ayoubi, S., Mokhtari, J., Mosaddeghi, M. R., & Zeraatpisheh, M. (2018a). Erodibility of calcareous soils as influenced by land use and intrinsic soil properties in a

semiarid region of central Iran. Environmental Monitoring and Assessment, 190(4), 192.

Ayoubi, S., Jabbari, M., & Khademi, H. (2018b). Multiple linear modeling between soil properties, magnetic susceptibility and heavy metals in various land uses. Modeling Earth Systems and Environment, 4(2), 579-589.

Bachmann, J., Ellies, A., & Hartge, K. (2000). Development and application of a new sessile drop contact angle method to assess soil water repellency. Journal of Hydrology, 231, 66-75.

Bisdom, E.B.A., Dekker, L.W., & Schoute, J. F. T. (1993). Water repellency of sieve fractions from sandy soils and relationships with organic material and soil structure. Geoderma, 56, 105-118.

Bryan, R. B. (2000). Soil erodibility and processes of water erosion on hillslope. Geomorphology, 32(3–4), 385-415.

Bryan, R.B., & Poesen, J.W.A. (1989). Laboratory experiments on the influence of slope length on runoff, percolation and rill development. Earth Surface Processes Landforms 14, 211–231.

British Standards Institution. (1990). BS 1377:1990. Methods of test for soils for civil engineering purposes.

Carollo, F. G., Ferro, V., & Serio, M. A. (2017). Reliability of rainfall kinetic power–intensity relationships. Hydrological Processes, 31(6), 1293-1300.

Cerdà, A., Schnabel, S., Ceballos, A., & Gomez-Amelia, D. (1998). Soil hydrological response under simulated rainfall in the Dehesa land system (Extremadura, SW

723 Spain) under drought conditions. Earth Surface Processes and Landforms, 23(3),
724 195-209.
725 Dell'Avanzi, E., Guizelini, A., da Silva, W., & Nocko, L. (2010). Potential use of
726 induced soil-water repellency techniques to improve the performance of landfill's
727 alternative final cover systems. Unsaturated soils. CRC Press, Boca Raton, FL,
728 461-466.
729 Doerr, S. H. (1998). On standardizing the 'water drop penetration time' and the
730 'molarity of an ethanol droplet' techniques to classify soil hydrophobicity: a case
731 study using medium textured soils. Earth Surface Processes and Landforms,
732 23(7), 663-668.
733 Doerr, S. H., Shakesby, R. A., Blake, W. H., Chafer, C. J., Humphreys, G. S., &
734 Wallbrink, P. J. (2006). Effects of differing wildfire severities on soil wettability and
735 implications for hydrological response. Journal of Hydrology, 319(1-4), 295-311.
736 Ebel, B. A., & Moody, J. A. (2017). Synthesis of soil-hydraulic properties and
737 infiltration timescales in wildfire-affected soils. Hydrological Processes, 31(2),
738 324-340.
739 Fox, G. A., & Wilson, G. V. (2010). The role of subsurface flow in hillslope and stream
740 bank erosion: A review. Soil Science Society of America Journal, 74(3), 717-733.
741 Fox, D. M., Darboux, F., & Carrega, P. (2007). Effects of fire-induced water repellency
742 on soil aggregate stability, splash erosion, and saturated hydraulic conductivity for
743 different size fractions. Hydrological Processes, 21(17), 2377-2384.

744 Greene, R. S. B., & Hairsine, P. B. (2004). Elementary processes of soil-water
745 interaction and thresholds in soil surface dynamics: A review. Earth Surface
746 Processes and Landforms, 29(9), 1077-1091.
747 Jordán, A., Zavala, L. M., Granged, A. J. P., Gordillo-Rivero, Á. J., García-Moreno, J.,
748 Pereira, P., . . . Alanís, N. (2016). Wettability of ash conditions splash erosion and
749 runoff rates in the post-fire. Science of The Total Environment, 572, 1261-1268.
750 Knapen, A., Poesen, J., Govers, G., Gyssels, G., & Nachtergaele, J. (2007).
751 Resistance of soils to concentrated flow erosion: A review. Earth-Science
752 Reviews, 80(1), 75-109.
753 Larsen, I. J., MacDonald, L. H., Brown, E., Rough, D., Welsh, M. J., Pietraszek, J.
754 H., . . . Schaffrath, K. (2009). Causes of post-fire runoff and erosion: Water
755 repellency, cover, or soil sealing? Soil Science Society of America Journal, 73(4),
756 1393-1407.
757 Leelamanie, D., Karube, J., & Yoshida, A. (2008). Characterizing water repellency
758 indices: Contact angle and water drop penetration time of hydrophobized sand.
759 Soil Science & Plant Nutrition, 54(2), 179-187.
760 Leighton-Boyce, G., Doerr, S. H., Shakesby, R. A., & Walsh, R. P. D. (2007).
761 Quantifying the impact of soil water repellency on overland flow generation and
762 erosion: A new approach using rainfall simulation and wetting agent on in situ soil.
763 Hydrological Processes, 21(17), 2337-2345.
764 Lourenço, S. D. N., Saulick, Y., Zheng, S., Kang, H., Liu, D., Lin, H., & Yao, T. (2018).
765 Soil wettability in ground engineering: fundamentals, methods, and applications.

766 Acta Geotechnica, 13(1), 1-14.
767 Mao, J., Nierop, K. G. J., Dekker, S. C., Dekker, L. W., & Chen, B. (2019).
768 Understanding the mechanisms of soil water repellency from nanoscale to
769 ecosystem scale: a review. Journal of Soils and Sediments, 19(1), 171-185.
770 McHale, G., Shirtcliffe, N. J., Newton, M. I., & Pyatt, F. B. (2007). Implications of ideas
771 on super-hydrophobicity for water repellent soil. Hydrological Processes, 21(17),
772 2229-2238.
773 Mohammadi, S., Homaee, M., & Sadeghi, S. H. (2018). Runoff and sediment behavior
774 from soil plots contaminated with kerosene and gasoil. Soil and Tillage Research,
775 182, 1-9.
776 Nearing, M. A., Yin, S.-q., Borrelli, P., & Polyakov, V. O. (2017). Rainfall erosivity: An
777 historical review. Catena, 157, 357-362.
778 Ng, S. H. Y., & Lourenço, S. D. N. (2016). Conditions to induce water repellency in
779 soils with dimethyldichlorosilane. Géotechnique, 66(5), 441-444.
780 Osborn, J.R., Pelishek, R.E., Krammes, J.S., & Letey, J. (1964). Soil wettability as a
781 factor in erodibility. Soil Science Society of America Proceedings, 28(2), 294–295.
782 Powell, D. M. (2014). Flow resistance in gravel-bed rivers: Progress in research.
783 Earth-Science Reviews, 136, 301-338.
784 Rahimi, M. R., Ayoubi, S., & Abdi, M. R. (2013). Magnetic susceptibility and Cs-137
785 inventory variability as influenced by land use change and slope positions in a
786 hilly, semiarid region of west-central Iran. Journal of Applied Geophysics, 89,
787 68-75.

788 Renard, K. G., Foster, G. R., Weesies, G. A., & Porter, J. P. (1991). RUSLE: Revised
789 universal soil loss equation. Journal of Soil and Water Conservation, 46(1), 30-33.
790 Saulick, Y., Lourenço, S. D. N., & Baudet, B. A. (2017). A semi-automated technique
791 for repeatable and reproducible contact angle measurements in granular
792 materials using the sessile drop method. Soil Science Society of America Journal,
793 81(2), 241-249.
794 Saulick, Y., Lourenço, S. D. N., Baudet, B. A., Woche, S. K., & Bachmann, J. (2018).
795 Physical properties controlling water repellency in synthesized granular solids.
796 European Journal of Soil Science, 69(4), 698-709.
797 Shakesby, R. A., Coelho, C. D. O. A., Ferreira, A. D., Terry, J. P., & Walsh, R. P. (1993).
798 Wildfire impacts on soil erosion and hydrology in wet Mediterranean forest,
799 Portugal. International Journal of Wildland Fire, 3(2), 95-110.
800 Sharma, P. P., Gupta, S. C., & Rawls, W. J. (1991). Soil detachment by single
801 raindrops of varying kinetic energy. Soil Science Society of America Journal,
802 55(2), 301-307.
803 Sheridan, G.J., So, H.B., Loch, R.J., Pocknee, C., & Walker, C.M. (2000). Use of
804 laboratory-scale rill and interrill erodibility measurements for the prediction of
805 hillslope-scale erosion on rehabilitated coal mine soils and overburdens.
806 Australian Journal of Soil Research 38, 285–297.
807 Sheridan, G. J., Lane, P. N. J., & Noske, P. J. (2007). Quantification of hillslope runoff
808 and erosion processes before and after wildfire in a wet Eucalyptus forest.
809 Journal of Hydrology, 343(1–2), 12-28.

Shi, P., Arter, C., Liu, X., Keller, M., & Schulin, R. (2017). Soil aggregate stability and size-selective sediment transport with surface runoff as affected by organic residue amendment. Science of The Total Environment, 607-608, 95-102.

Tajik, S., Ayoubi, S., & Nourbakhsh, F. (2012). Prediction of soil enzymes activity by digital terrain analysis: comparing artificial neural network and multiple linear regression models. Environmental Engineering Science, 29(8), 798-806.

Tarchitzky, J., Lerner, O., Shani, U., Arye, G., Lowengart-Aycicegi, A., Brener, A., & Chen, Y. (2007). Water distribution pattern in treated wastewater irrigated soils: Hydrophobicity effect. European Journal of Soil Science, 58(3), 573-588.

Terry, J. P., & Shakesby, R. A. (1993). Soil hydrophobicity effects on rainsplash: Simulated rainfall and photographic evidence. Earth Surface Processes and Landforms, 18(6), 519-525.

Torfs, H., Jiang, J., & Mehta, A. J. (2000). Assessment of the erodibility of fine/coarse sediment mixtures. In W. H. McAnally & A. J. Mehta (Eds.), Proceedings in Marine Science (Vol. 3, pp. 109-123): Elsevier.

van Dijk, A. I. J. M., Bruijnzeel, L. A., & Rosewell, C. J. (2002). Rainfall intensity - kinetic energy relationships: a critical literature appraisal. Journal of Hydrology, 261(1), 1-23.

Wang, Z., Wu, L., & Wu, Q. (2000). Water-entry value as an alternative indicator of soil water-repellency and wettability. Journal of Hydrology, 231, 76-83.

Wischmeier, W. H., & Mannering, J. (1969). Relation of soil properties to its erodibility. Soil Science Society of America Journal, 33(1), 131-137.

832 Zaiontz, C. (2018). Real Statistics Using Excel. www.real-statistics.com (accessed on
833 11 September 2018).
834 Zheng, S., Lourenço, S. D. N., Cleall, P. J., Chui, T. F. M., Ng, A. K. Y., & Millis, S. W.
835 (2017). Hydrologic behavior of model slopes with synthetic water repellent soils.
836 Journal of Hydrology, 554, 582-599.

837 **Captions of figures and tables**

838

839 Table 1: Physical properties of Fujian sand and crushed silica.

840 Table 2: Summary of settings and results of flume test, where α denotes contact angle;
841 i denotes rainfall intensity; S_a denotes average sediment concentration; S_p
842 denotes peak sediment concentration; T_p denotes time to peak sediment; E_s
843 denotes splash erosion rate. Statistically significant differences between
844 experiments ($p < 0.05$) are denoted by superscript letters (a, b, c etc.), values with
845 the same superscript letters mean that no statistically significant differences were
846 observed for these experiments.

847 Table 3: Correlation matrix for contact angle, rainfall intensity and erosional variables
848 (Fujian sand and sand/silt mixture), where α denotes contact angle; i denotes
849 rainfall intensity; S_a denotes average sediment concentration; S_p denotes peak
850 sediment concentration; T_p denotes time to peak sediment.

851

852 Figure 1: Schematic illustration of flume dimension and instrumentation.

853 Figure 2: Time series data for wettable and subcritical water repellent sand (test 7). (a)
854 Runoff rate and sediment concentration. (b) Volumetric water content at various
855 locations. (c) Surface morphology evolution, where the surface morphology
856 features were outlined by dotted lines.

857 Figure 3: Time series data for water repellent sand (test 3). (a) Runoff rate and
858 sediment concentration. (b) Volumetric water content at various locations. (c)

Surface morphology evolution, where the surface morphology features were outlined by dotted lines.

Figure 4: Time series data for wettable sand/silt mixture (test 16). (a) Runoff rate and sediment concentration. (b) Volumetric water content at various locations. (c) Surface morphology evolution, where the surface morphology features were outlined by dotted lines.

Figure 5: Time series data for subcritical water repellent sand/silt mixture. (a) Runoff rate and sediment concentration (test 23). (b) Volumetric water content at various locations (test 23). (c) Surface morphology evolution (test 5), where the surface morphology features were outlined by dotted lines.

Figure 6: Time series data for water repellent sand/silt mixture (test 6). (a) Runoff rate and sediment concentration. (b) Volumetric water content at various locations. (c) Surface morphology evolution, where the surface morphology features were outlined by dotted lines.

Figure 7: Summary of erosional variables in flume tests: Time to peak sediment of (a) sand and (b) sand/silt mixture; Average sediment concentration of (c) sand and (d) sand/silt mixture; Peak sediment concentration of (e) sand and (f) sand/silt mixture; Total mass of sediment of (g) sand and (h) sand/silt mixture; Time to peak runoff of (i) sand and (j) sand/silt mixture.

Figure 8: Summary of splash erosion rate of (a) sand and (b) sand/silt mixture. The ends of the box are the upper and lower quartiles, the median is marked by a solid line inside the box, and the mean is marked by a cross inside the box, the

whiskers are the two lines outside the box that extend to the highest and lowest values observed.

Figure 9: Summary of temporal change in D_{60} of sediment for (a) sand and (b) sand/silt mixture.

Figure 10: Hydraulically smooth flow and rough flow on sand/silt mixture and Fujian sand. *after* Powell (2014).

Figures and Tables

Properties	Fujian sand	crushed silica
Specific gravity, G_s	2.66	2.68
Maximum void ratio, e_{max}	0.56	1.74
Minimum void ratio, e_{min}	0.42	0.68
Coefficient of uniformity, Cu	5.56	2.80
Coefficient of curvature, Cc	0.34	0.86
Organic matter content, %	0.16	0.52

Table 1: Physical properties of untreated Fujian sand and crushed silica.

Test No.	Test settings			Test results			
	α (°)	Grain size	i (mm/h)	S_a (g/L)	S_p (g/L)	T_p (min)	E_s (g/mm)
1	20	Sand	230	47.75^{abc}	75.78^{abcd}	25^{a}	0.04 ± 0.01^{abc}
2	90			40.78^{abc}	89.67^{abcd}	15^{a}	0.03 ± 0.01^{a}
3	120			94.81^{abc}	236.19^{bcd}	5^{a}	0.29 ± 0.08^{i}
4	20	Mixture		74.05^{abc}	160.81^{abcd}	15^{a}	0.06 ± 0.02^{abcd}
5	90			28.45^{abc}	89.01^{abcd}	2^{a}	0.11 ± 0.03^{def}
6	120			20.91^{abc}	74.12^{abcd}	4^{a}	0.20 ± 0.02^{ij}
7	20	Sand	170	23.90^{abc}	48.17^{abc}	20^{a}	0.09 ± 0.02^{cde}
8	90			44.29^{abc}	119.28^{abcd}	10^{a}	0.12 ± 0.02^{defg}
9	120			105.64^{bc}	162.45^{abcd}	20^{a}	0.27 ± 0.03^{kl}
10	20	Mixture		80.63^{abc}	223.66^{abcd}	15^{a}	0.08 ± 0.01^{bcde}
11	90			15.20^{abc}	61.53^{abc}	2^{a}	0.13 ± 0.01^{efgh}
12	120			13.69^{abc}	55.30^{abc}	4^{a}	0.13 ± 0.01^{efgh}
13	20	Sand	100	9.78^{ab}	17.87^{ab}	65^{ab}	0.01 ± 0.01^{a}
14	90			1.41^{a}	6.30^{ab}	5^{a}	0.03 ± 0.01^{a}
15	120			12.08^{ab}	16.60^{ab}	5^{a}	0.15 ± 0.03^{fghi}
16	20	Mixture		108.95^{c}	261.11^{cd}	20^{a}	0.01 ± 0.00^{a}
17	90			7.60^{ab}	35.67^{abc}	5^{a}	0.04 ± 0.01^{abc}
18	120			5.83^{a}	37.81^{abc}	5^{a}	0.17 ± 0.02^{ghij}
19	20	Sand	40	0.00^{a}	0.00^{a}	120^{b}	0.02 ± 0.01^{a}
20	90			0.05^{a}	0.38^{a}	70^{ab}	0.04 ± 0.02^{abc}
21	120			2.25^{a}	3.57^{ab}	60^{ab}	0.22 ± 0.06^{jk}
22	20	Mixture		83.49^{abc}	302.95^{d}	30^{a}	0.01 ± 0.01^{a}
23	90			6.37^{a}	17.85^{ab}	15^{a}	0.05 ± 0.02^{abc}
24	120			6.58^{ab}	20.22^{ab}	15^{a}	0.19 ± 0.03^{hij}

Table 2: Summary of settings and results of flume test, where α denotes contact angle; i denotes rainfall intensity; S_a denotes average sediment concentration; S_p denotes peak sediment concentration; T_p denotes time to peak sediment; E_s denotes splash erosion rate. Statistically significant differences between experiments ($p < 0.05$) are denoted by superscript letters (a, b, c etc.), values with the same superscript letters mean that no statistically significant differences were observed for these experiments.

	Fujian sand					sand/silt mixture				
	α	i	S_a	S_p	T_p	α	i	S_a	S_p	T_p
α	1					1				
i	0	1				0	1			
S_a	0.333	0.748**	1			-0.929**	0.068	1		
S_p	0.357	0.770**	0.951**	1		-0.892**	-0.017	0.958**	1	
T_p	-0.45	-0.687*	-0.501	-0.528	1	-0.714**	-0.560	0.696*	0.739**	1

* Correlation is significant at $p < 0.05$ level

** Correlation is significant at $p < 0.01$ level

Table 3: Correlation matrix for contact angle, rainfall intensity and erosional variables (Fujian sand and sand/silt mixture), where α denotes contact angle; i denotes rainfall intensity; S_a denotes average sediment concentration; S_p denotes peak sediment concentration; T_p denotes time to peak sediment.

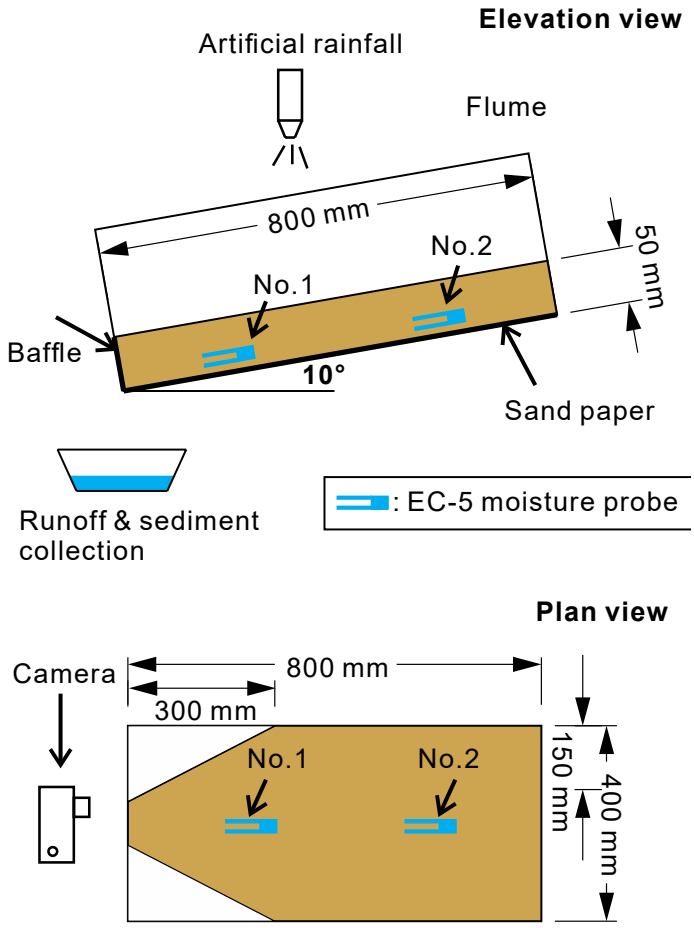

Figure 1: Schematic illustration of flume dimension and instrumentation.

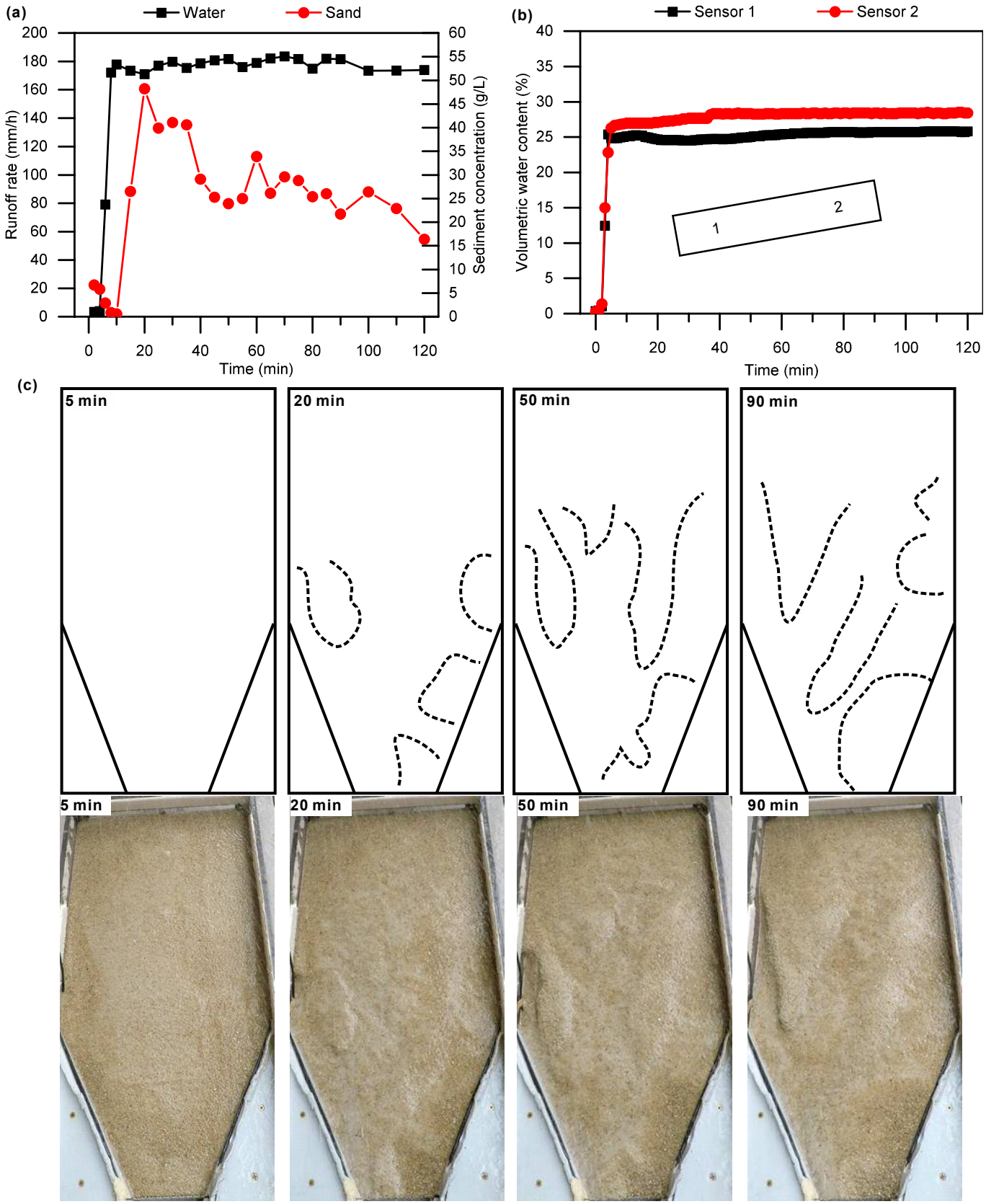

Figure 2: Time series data for wettable and subcritical water repellent sand (test 7). (a) Runoff rate and sediment concentration. (b) Volumetric water content at various locations. (c) Surface morphology evolution, where the surface morphology features were outlined by dotted lines.

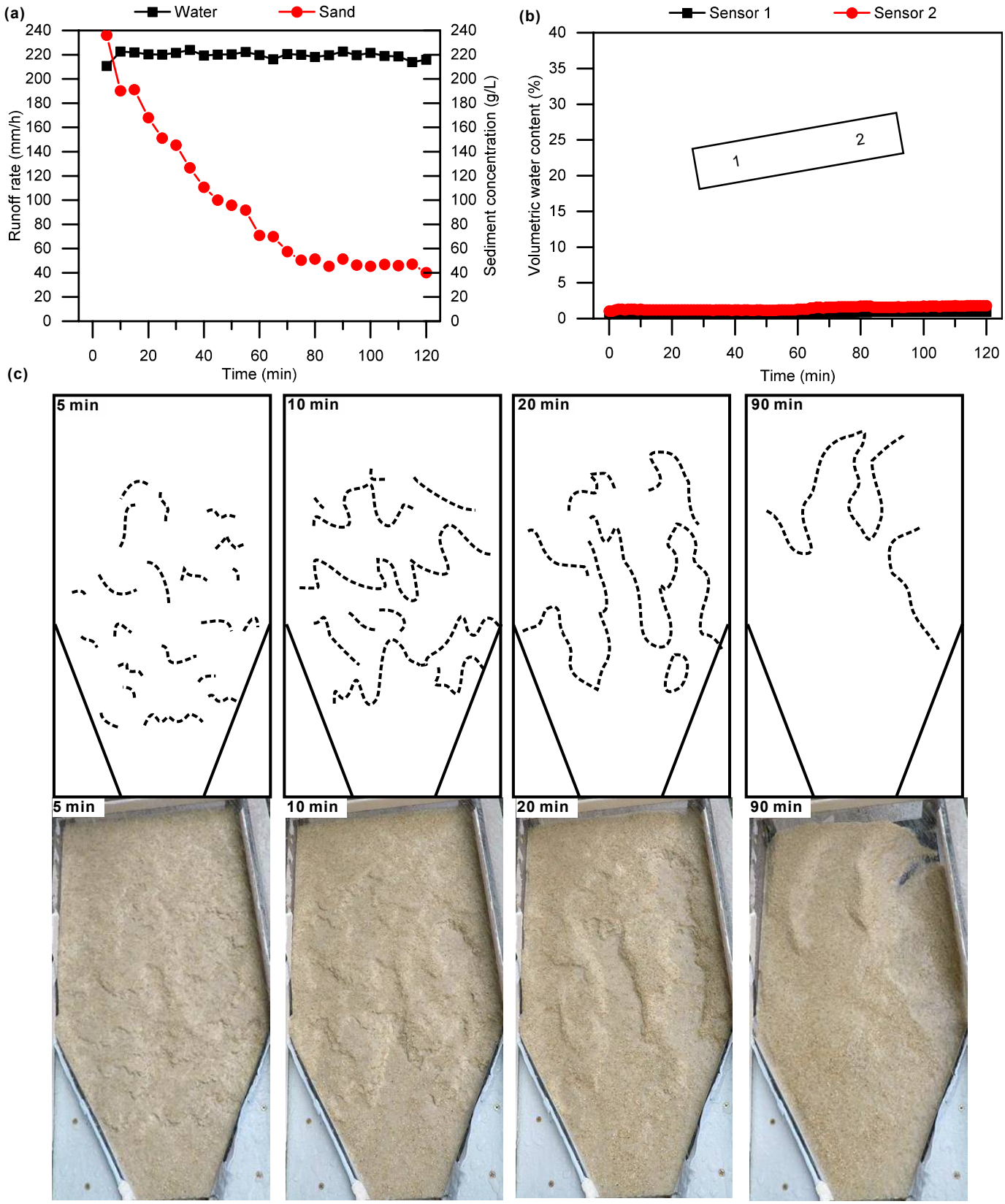

Figure 3: Time series data for water repellent sand (test 3). (a) Runoff rate and sediment concentration. (b) Volumetric water content at various locations. (c) Surface morphology evolution, where the surface morphology features were outlined by dotted lines.

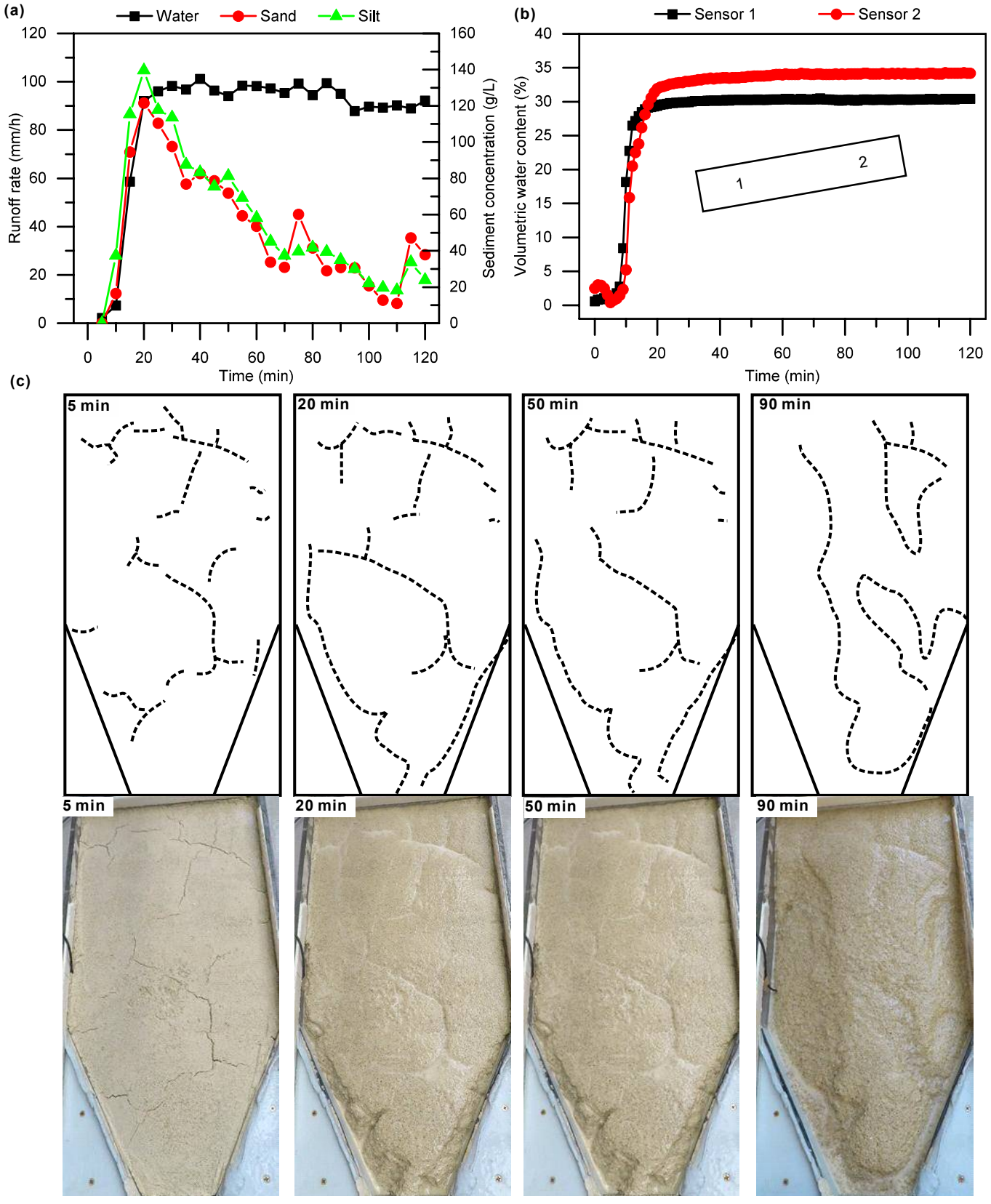

Figure 4: Time series data for wettable sand/silt mixture (test 16). (a) Runoff rate and sediment concentration. (b) Volumetric water content at various locations. (c) Surface morphology evolution, where the surface morphology features were outlined by dotted lines.

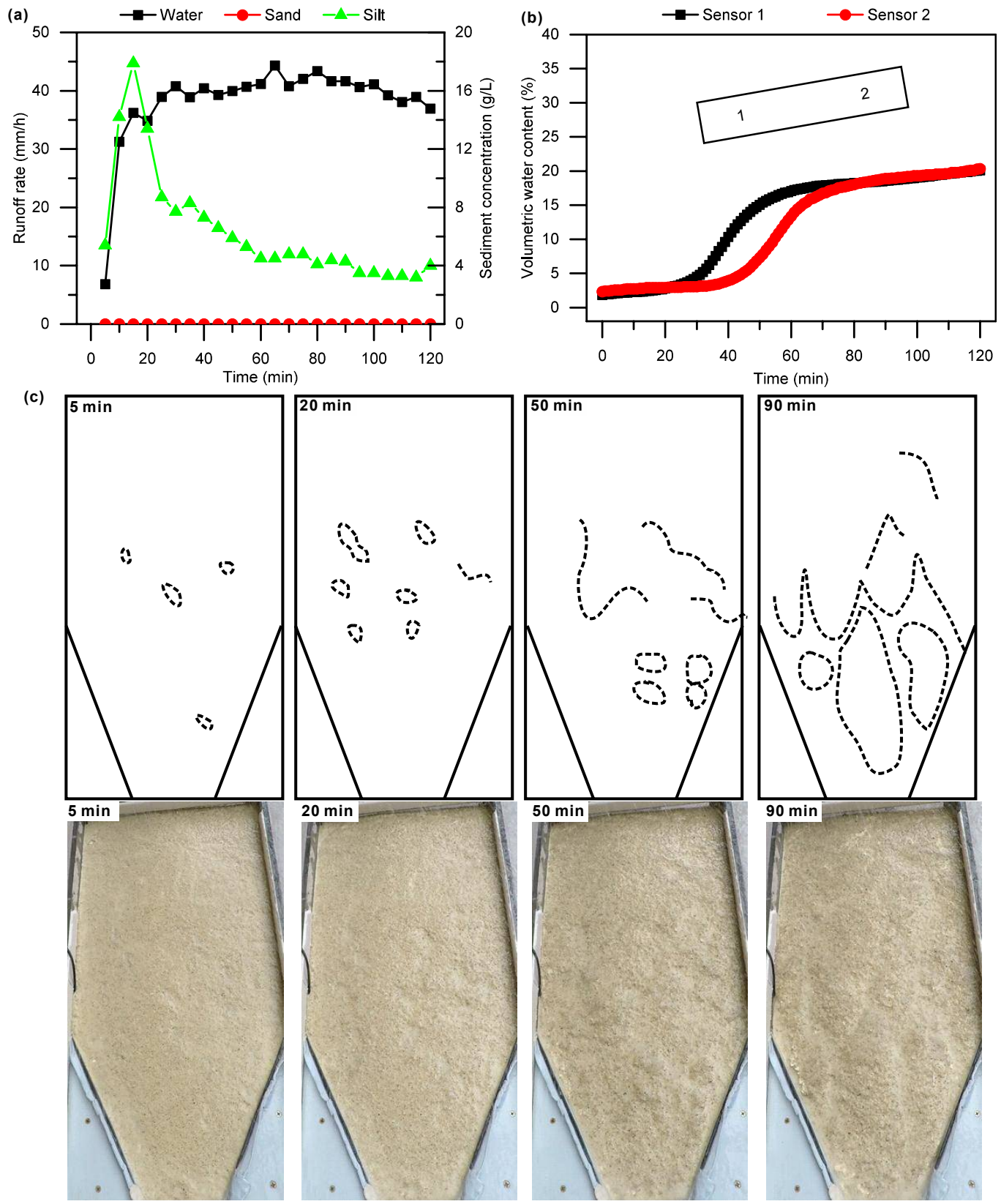

Figure 5: Time series data for subcritical water repellent sand/silt mixture. (a) Runoff rate and sediment concentration (test 23). (b) Volumetric water content at various locations (test 23). (c) Surface morphology evolution (test 5), where the surface morphology features were outlined by dotted lines.

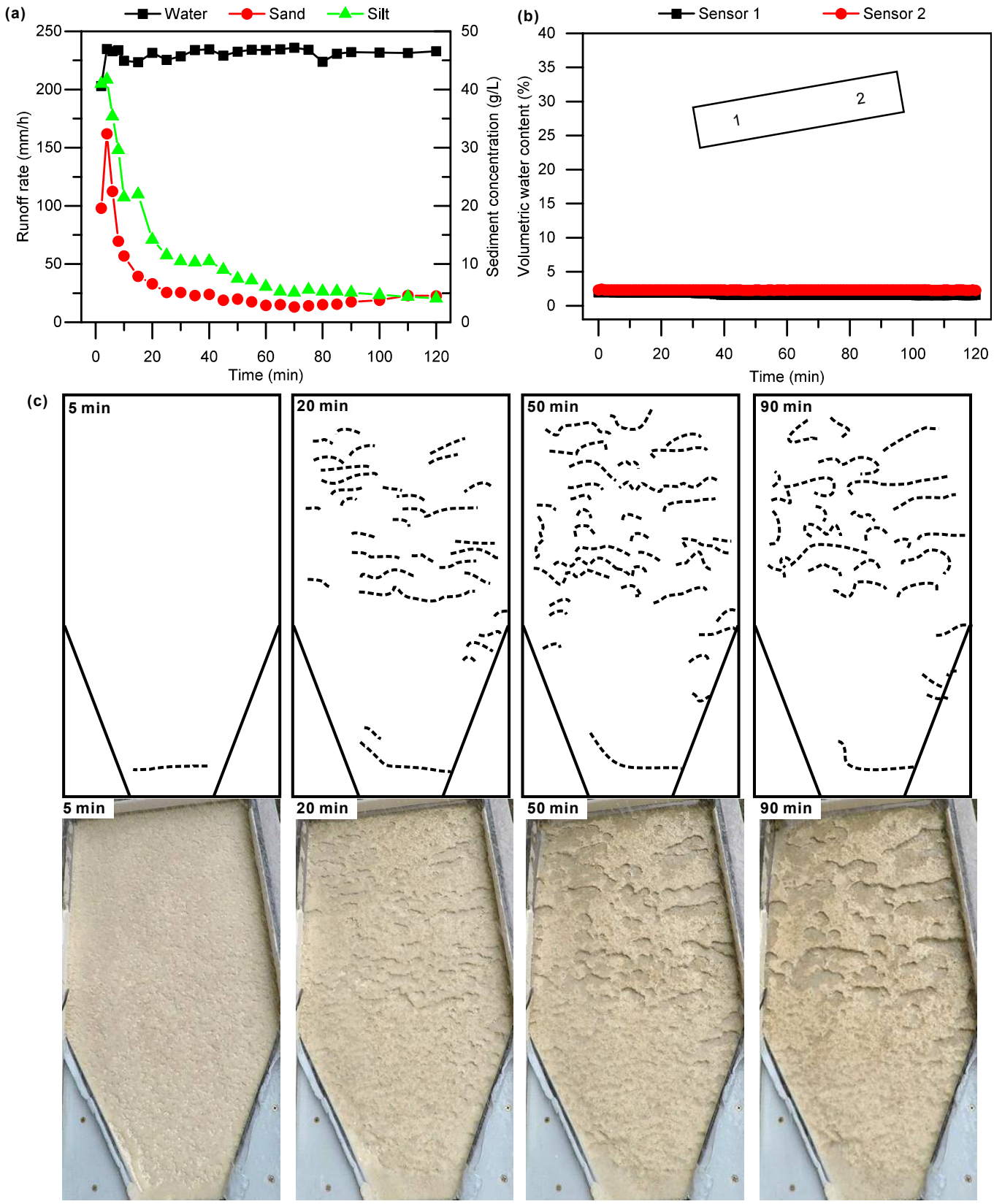

Figure 6: Time series data for water repellent sand/silt mixture (test 6). (a) Runoff rate and sediment concentration. (b) Volumetric water content at various locations. (c) Surface morphology evolution, where the surface morphology features were outlined by dotted lines.

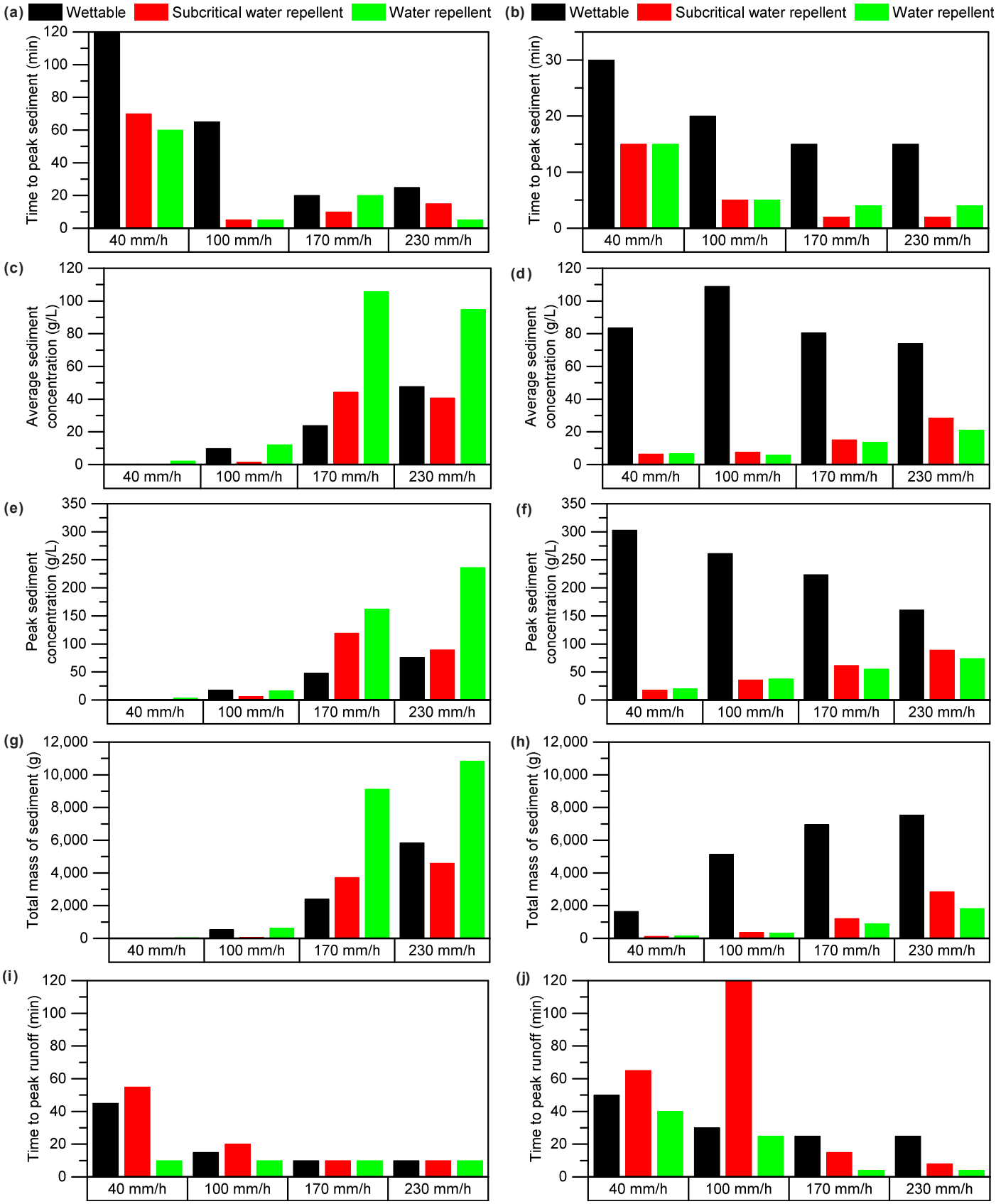

Figure 7: Summary of erosional variables in flume tests: Time to peak sediment of (a) sand and (b) sand/silt mixture; Average sediment concentration of (c) sand and (d) sand/silt mixture; Peak sediment concentration of (e) sand and (f) sand/silt mixture; Total mass of sediment of (g) sand and (h) sand/silt mixture; Time to peak runoff of (i) sand and (j) sand/silt mixture.

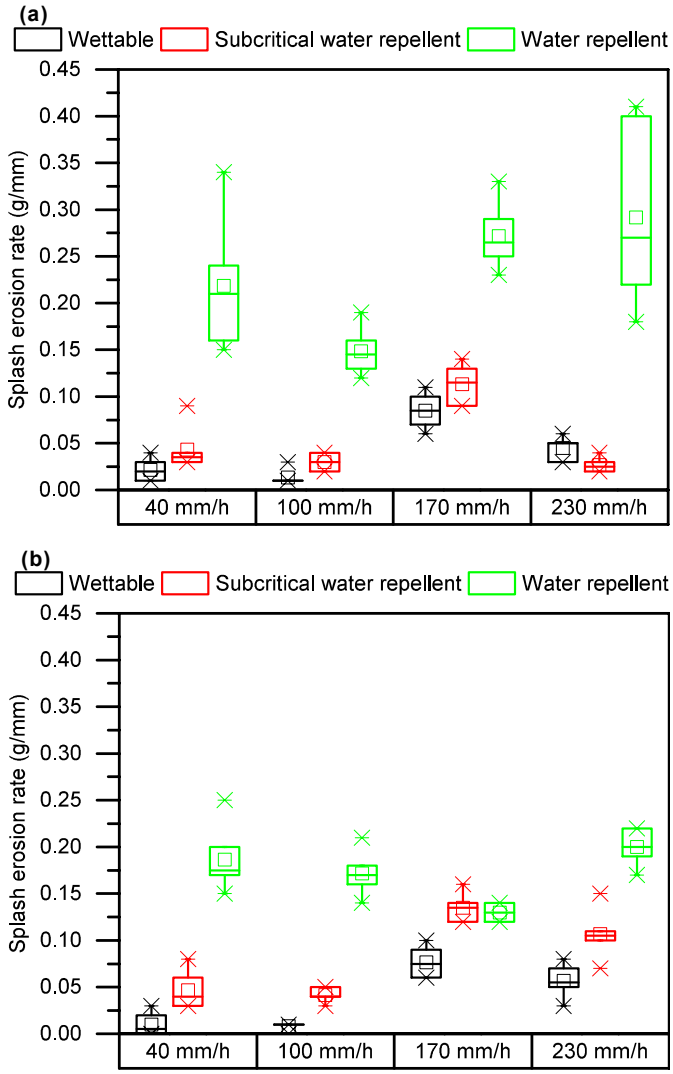

Figure 8: Summary of splash erosion rate of (a) sand and (b) sand/silt mixture. The ends of the box are the upper and lower quartiles, the median is marked by a solid line inside the box, and the mean is marked by a cross inside the box, the whiskers are the two lines outside the box that extend to the highest and lowest values observed.

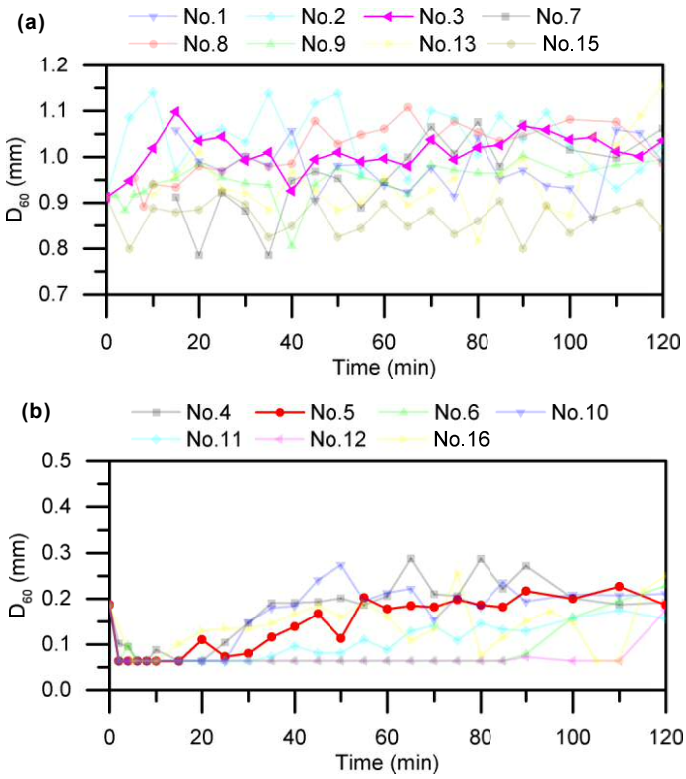

Figure 9: Summary of temporal change in D_{60} of sediment for (a) sand and (b) sand/silt mixture.

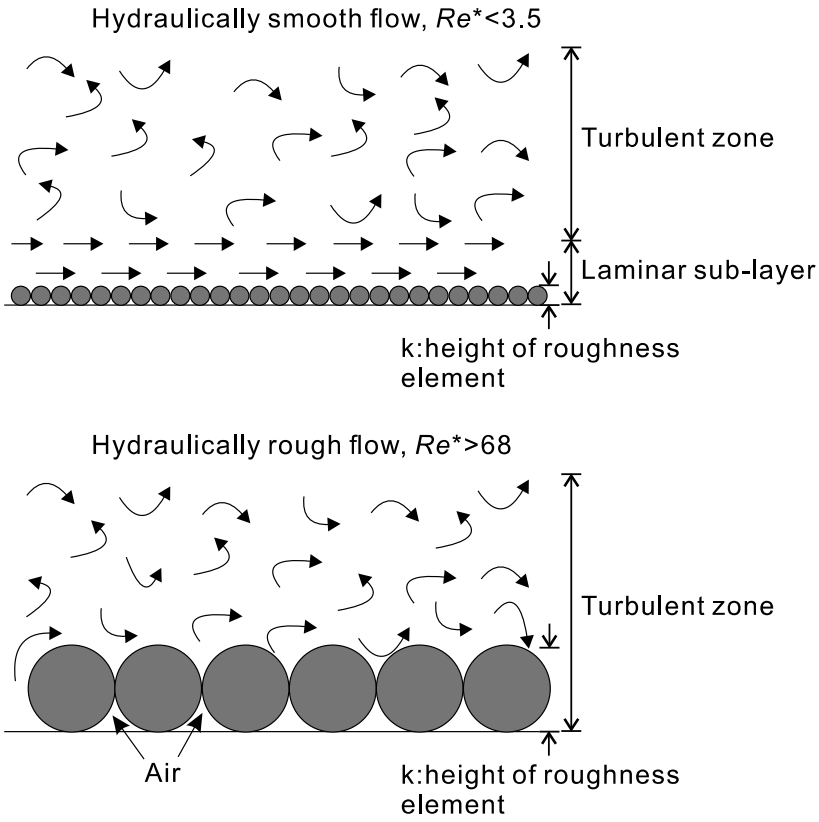

Figure 10: Hydraulically smooth flow and rough flow on sand/silt mixture and Fujian sand. *after* Powell (2014).

Supplementary materials:

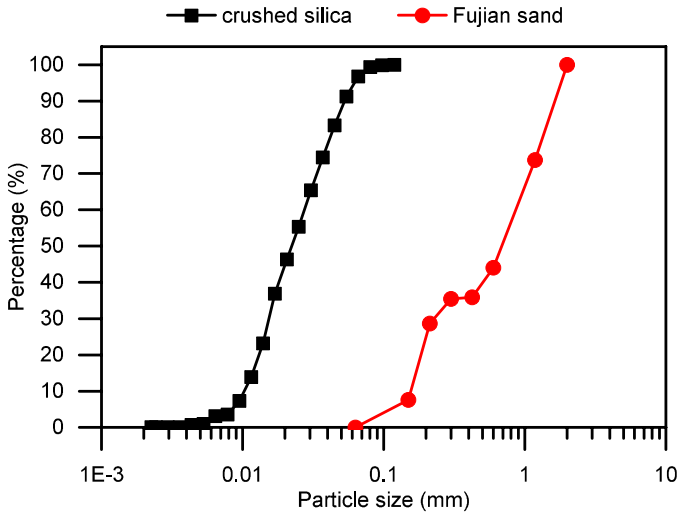

Figure S1: Particle size distributions of Fujian sand and crushed silica.

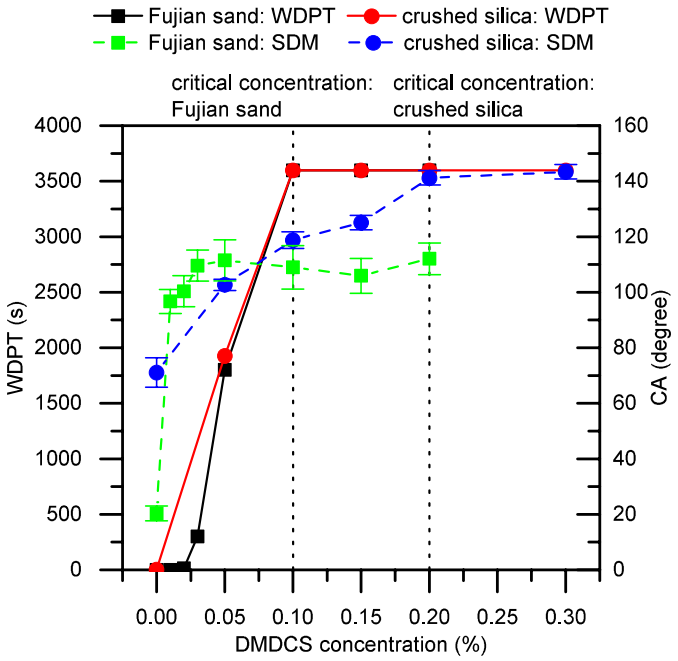

Figure S2: WDPT and CA for Fujian sand and crushed silica with various DMDCS concentration.